International Communications in Heat and Mass Transfer 120 (2021) 105019

Contents lists available at ScienceDirect

International Communications in Heat and Mass Transfer

journal homepage: www.elsevier.com/locate/ichmt

Self-activated elastocapillary wave promotes boiling heat transfer on soft liquid metal surface

Chunlei Cao [a], Xiaojing Ma [a], Xiaotian He [a], Jinliang Xu [a,*], Jian Xie [b,*], Guohua Liu [b]

[a] Beijing Key Laboratory of Multiphase Flow and Heat Transfer for Low Grade Energy Utilization, North China Electric Power University, Beijing 102206, China
[b] Key Laboratory of Power Station Energy Transfer Conversion and System of Ministry of Education, North China Electric Power University, Beijing 102206, China

ARTICLE INFO

Keywords:
Boiling
Soft surface
Elasocapillary wave
Superheating boundary layer

ABSTRACT

Current studies use stiff micro/nano structure to augment boiling heat transfer, there is a superheating boundary layer near the hard structure to dominate the boiling process. Here, comparative studies were performed for pool boiling of ethanol on a hard copper surface and a ~100 μm soft Galinstan liquid metal surface. The latter behaves significant heat transfer enhancement, which is more evident for saturated boiling, under which heat transfer coefficients are raised by 60.5% compared to bare copper surface, maximally. The soft surface decreases bubble departure size by half, and increases bubble departure frequency by ~7 times. These distinct characteristics of bubble dynamics result in the decrease of wall superheating at onset of nucleate boiling from ~13 K on hard copper surface to ~5 K on soft surface. Elastocapillary wave and dynamic wrinkles are observed to disturb the near wall boundary layer for heat transfer enhancement, which are formed by the energy and force interactions between departing bubbles and soft liquid metal. The easier bubble nucleation on soft surface agrees with the bubble nucleation theory for a system including two immiscible liquids. Our study provides an alternative way using self-activated elastocapillary wave to promote boiling heat transfer.

1. Introduction

For a long history, mankind observed that solid can be deformed when compression is exerted on a soft material. Fundamental studies on the deformation of soft materials have only been received attention in the past two decades [1–3]. When the three phases of solid, liquid and gas meet at the contact line, the well-known Young equation gives $\cos\theta = (\gamma_{sv} - \gamma_{sl})/\gamma_{lv}$, where θ is the contact angle, γ is the surface tension, the subscripts of s, v and l represent solid, vapor and liquid, respectively. Even though the Young equation has been widely used, one notes that the equation emphasizes the force balance along the surface plane, but the vertical component of the surface tension is neglected. The latter plays key role in deforming a soft solid near the three-phase contact line [3–5]. The elastocapillary length is expressed as $l_{ec} = \gamma_{lv}/\mu$, characterizing the relative importance of surface tension of liquid and vapor relative to the elasticity of soft solid μ. The elastocapillary effect is important when the characteristic length of soft solid is smaller than l_{ec}. Crease and wrinkle are two types of deformation [6–8]. The elastocapillary induced deformation and instability are related to the wrapping of a liquid drop by a thin elastic film [9], coalescence of thin wet fibers [10,11], cavitation in soft hydrogel [12], formation of dynamic patterns on curved surface [13] to name a few.

The elastocapillary effect for droplet interacting with soft solid have been widely investigated [1,3,9,14,15]. Bubbles are more active than droplet, thus the elastocapillary effect with bubbles in the system is less reported. Boiling is phase-change heat transfer process governed by the bubble dynamics. The elastocapillary effect is also seldom considered in boiling heat transfer. Currently, boiling on solid surface use stiff micro/nano structures to promote the heat transfer performance [16–18], including micro-pin-fin, nanoparticles and porous materials, etc. There is a superheating liquid boundary layer on solid surface. Transient conduction, microconvection and microlayer evaporation in the superheating boundary layer are the mechanisms for boiling [19].

As a soft material, liquid metal is introduced in boiling system in this paper. In contrast to the three-phase system of solid, liquid and vapor, boiling on a liquid metal surface involves two-phases of liquid and vapor, but liquid contains two components including a deformable liquid metal and a boiling liquid such as ethanol. We show that, compared to hard copper surface, liquid metal obviously reduces wall superheating at the onset of nucleate boiling (ONB). Most importantly, bubble nucleation, growth and departure create dynamic wrinkles and elastocapillary wave of liquid metal. In turn, this interface instability

* Corresponding authors.
E-mail addresses: xjl@ncepu.edu.cn (J. Xu), xiejian90@ncepu.edu.cn (J. Xie).

https://doi.org/10.1016/j.icheatmasstransfer.2020.105019

Available online 16 November 2020

reduces the superheating boundary layer thickness of boiling liquid, thus boiling heat transfer is augmented.

2. Experiment

Comparative experiments were performed on hard copper surface (CS) and soft Galinstan liquid metal surface (SS) at atmospheric pressure. The test surface was a circle with a diameter of 10.0 mm, pool liquid temperatures were $T_b = 78$ °C, 60 °C and 40 °C, and ethanol was the boiling liquid. The details of test section, experiment setup, surface characterization and data reduction are as follows.

2.1. Test section

The copper block test section is shown in Fig. 1a. Four test sections were fabricated, one for boiling on copper surface, and the other three for boiling on soft Galinstan surface. All cooper blocks had a 48 mm height, having a footprint area of 47 mm × 50 mm. For each test section, four cartridge heaters were inserted in 8.0 mm diameter holes at the copper block bottom, each having a maximum power of 150 W at an AC (alternative current) voltage of 220 V. The middle part of the copper block had three 1.0 mm diameter holes. Three K-type thermocouples were inserted in these miniature holes. The copper block had a circular surface with a diameter of 10.0 mm, which was exposed in ethanol liquid in experiment.

Before formal experiment, the test surface was sand polished, and consecutively rinsed by dilute muriatic acid and acetone using ultrasonic vibration technique. After that, the copper surface was clean and ready for experiment. For boiling experiment on soft liquid surface, a Galinstan droplet was dripped on copper surface in pool ethanol liquid

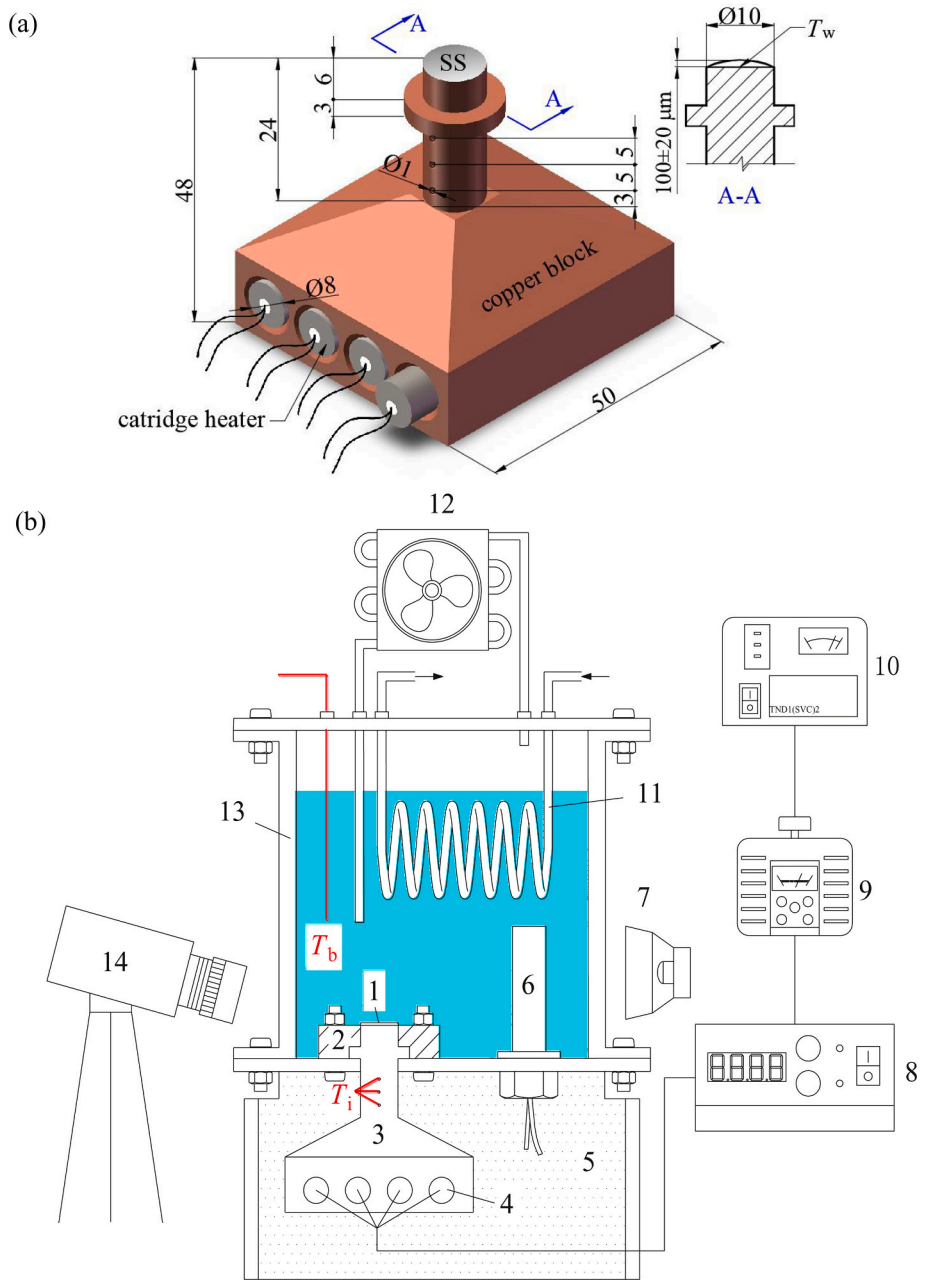

Fig. 1. Test section (a) and pool boiling experiment setup (all dimensions are in mm; 1: $Ga_{68.5}In_{21.5}Sn_{10}$; 2: teflon; 3: copper block; 4: cartridge heater; 5: insulation material; 6: auxiliary heater; 7: lamp; 8: power meter; 9: voltage transformer; 10: voltage stabilizer; 11: coiled-tube;12: air-cooled condenser; 13: tempered glass; 14: high-speed camera)

environment, preventing Galinstan from oxidation. Because copper is hydrophilic to Galinstan, the liquid metal quickly spreads on the copper surface to form a soft liquid film. During whole experiment, the liquid metal was not exposed in air to prevent oxidation. The deposited liquid mass of Galinstan was well controlled and determined by the weight difference of the dripping tube before and after deposition. In our experiment, three pool liquid temperatures of T_b = 78 °C, 60 °C and 40 °C were used. For each T_b experiment, a fresh copper block test section was used and deposited by soft liquid metal on top surface. The thickness of the liquid metal was estimated as 101.3 μm, 101.9 μm and 101.5 μm for boiling experiments with T_b = 78 °C, 60 °C and 40 °C, respectively.

2.2. Experimental setup

Fig. 1b shows the experiment setup. The test surface and ethanol were enclosed in a transparent glass chamber. There was a stainless-steel plate on the bottom of the glass chamber. A circular hole was at the stainless-steel plate center to fit the copper block. Teflon was adapted between the stainless-steel plate and the copper block. Epoxy glue was filled for seal. The heater surface was immersed by pool ethanol. The main body of the copper block outside of the glass chamber was insulated by a thermal insulation material. During experiment, the glass chamber was kept at atmospheric pressure. The power supply system included a 220 V voltage stabilizer, a voltage transformer and a power-meter. The latter gave the power reading. All temperatures were recorded by a Hewlett–Packard data acquisition system. A high-speed camera collected the boiling patterns. To observe the elastocapillary wave propagation on the soft surface during boiling, high recording rate such as 4000 images per second was used. The pool liquid temperature was well controlled, by applying a vapor condenser outside of the glass chamber, and a coiled copper tube and an auxiliary heater inside the glass chamber. The tap water was flowing inside the capillary tube. In such a way, the pool liquid temperature was controlled with an uncertainty of 0.3 °C. The following experiment procedures were applied:

- ✓ Turn on cartridge heaters to boil ethanol for our hour to remove non-condensable gas in liquid. Experiment started from a very small heat flux such as q = 0.5 W/cm^2.
- ✓ Setup a desired pool liquid temperature T_b. If T_b was smaller than the desired value, the auxiliary heater was turned on, alternatively, the auxiliary heater was turned off but the tap water flow rate was adjusted, until the desired T_b was reached.
- ✓ Collect data when steady experiment state was reached.
- ✓ Increase heat flux on heater surface and repeat the above procedures.
- ✓ Experiment was stopped when critical heat flux was reached.

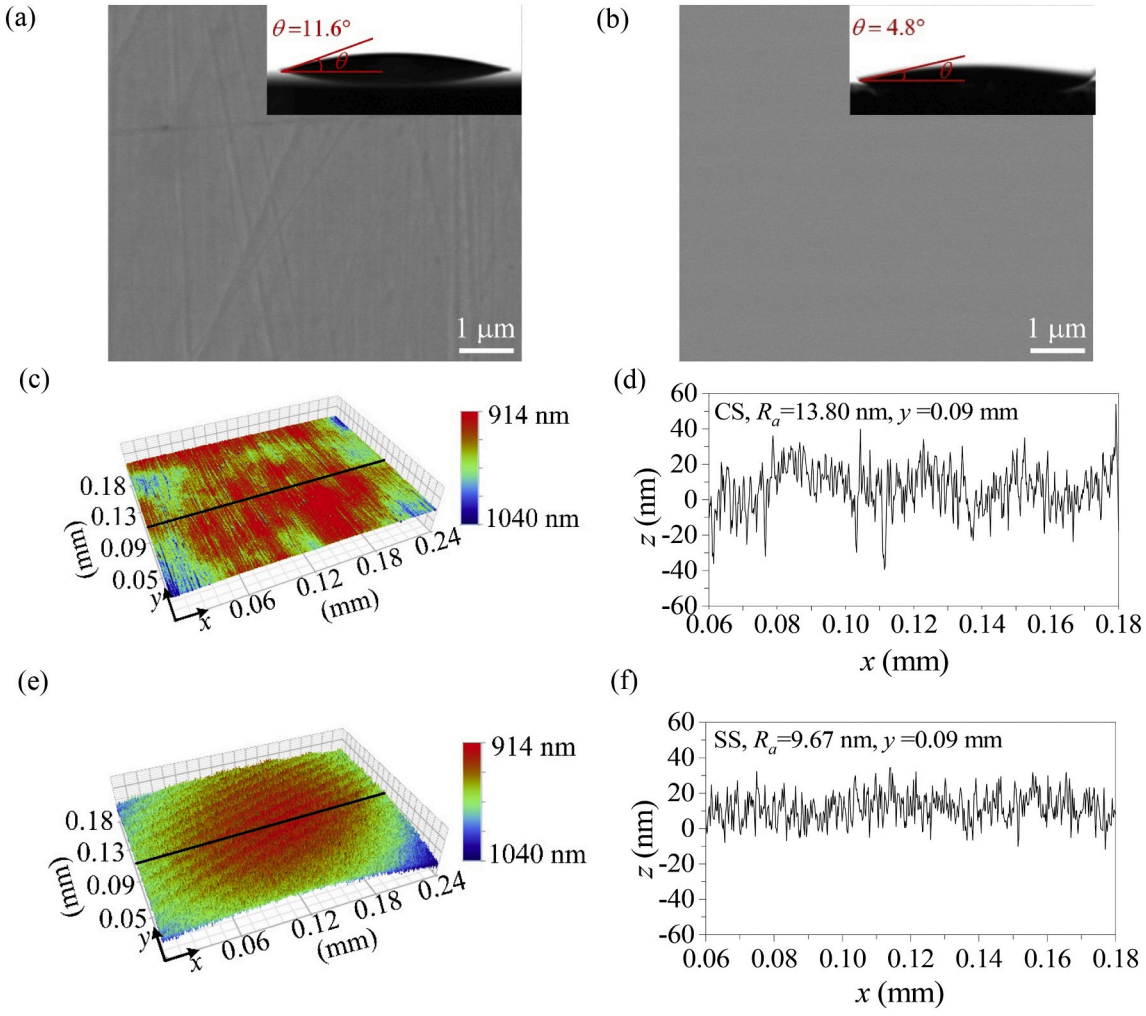

Fig. 2. The surface characterization and morphology (a: polished copper surface with contact angle of 11.6°; b: Galinstan surface measured by environmental scanning electronic microscope ESEM (FEI, Quanta 200, USA), with contact angle of 4.8° measured by contact angle instrument (Dataphysics OCA15 plus, GER); c-f: surface morphology measured by 3D optical microscope (Bruker, ContourGT-K, USA) with an uncertainty of 0.3 nm, c & d are for copper surface, e & f are for liquid metal surface.)

2.3. Surface characterization and physical properties

Before boiling experiment, the test surfaces were prepared and characterized (see Fig. 2). The sand polished copper surface and Galinstan surface were characterized by an environmental scanning electronic microscope ESEM (FEI, Quanta 200, USA), with a magnifying factor of 40,000 and a resolution of 3.7 nm. The surface morphology was measured by a 3D optical microscope (Bruker, ContourGT-K, USA) with an uncertainty of 0.3 nm. Contact angles on the two surfaces were measured by Dataphysics (OCA15 plus, GER), with an uncertain of 0.1°. For contact angle measurement, we dripped an ethanol droplet with a ~ 2 mm diameter on the surface, and recorded the droplet morphology by a microscope. Processing the recorded image file with a digital image processing software obtains the contact angle value.

To characterize Before formal experiment, the test surface was sand polished, an *xy* plane was selected covering $x = 0.06$–0.18 mm and $y = 0.05$–0.18 mm. The roughness was characterized in *z* coordinate, which is perpendicular to the *xy* plane. The average roughness *Ra* is defined as $Ra = \frac{1}{l_x}\int_0^{l_x}|z(x)|dx$, where $l_x = 0.18$ mm here. Another parameter is the peak-valley roughness $Rt = Rp + Rv$, where *Rp* and *Rv* are the peak value and valley value, respectively. Above the average roughness, the peak value is $Rp_i = max[z(x)]$, $Rp = \frac{\sum_{i=1}^{n} Rp_i}{n}$, where *n* is the number of peaks. Alternatively, below the average roughness, the valley value is $Rv_i = |min[z(x)]|$, $Rv = \frac{\sum_{i=1}^{m} Rv_i}{m}$, where *m* is the number of valleys. In the present study, the sand polished copper surface (CS) had an average roughness $Ra = 13.8$ nm and a peak-valley roughness $Rt = 1954$ nm, with a contact angle of $\theta_{CS} = 11.6°$, which is hydrophilic to ethanol. Alternatively, compared to copper surface, the soft Galinstan surface (SS) had $Ra = 9.7$ nm and $Rt = 121$ nm, with a contact angle of $\theta_{SS} = 4.8°$, which is more hydrophilic to ethanol. Except the surface parameter of roughness and wettability, the involved physical properties of liquid metal and ethanol are list in Tables 1 and 2. Galinstan is a eutectic alloy containing the elements of gallium (Ga), indium (In) and stannum (Sn). The melting temperature of Galinstan is 10.5 °C [20]. The experiment was performed at a room temperature of about 26 °C, which is significantly higher than the melting temperature to ensure the liquid state of Galinstan. The boiling temperature of Galinstan is larger than 1300 °C [21]. Hence, it is impossible to boil or evaporate the Galinstan in the present experiment.

At atmospheric pressure and 20 °C, Galinstan has a low Prandtl number of 0.053, behaving faster heat diffusion compared to viscosity diffusion. This liquid metal has a thermal conductivity of 16.5 W/mK, which is 27.5 times of water at similar condition. A ~ 100 μm liquid metal was adhered on copper substrate. At heat flux $q = 100$ W/cm^2, the temperature difference across such liquid metal thickness is 3.9 K assuming heat conduction. The real temperature difference is much smaller than 3.9 K due to strong convection in liquid metal.

2.4. Data reduction and uncertainty analysis

The three jacket thermocouples shown in the cylinder part of Fig. 1a were marked as T_1, T_2 and T_3. The distance between two neighboring thermocouples was 5.0 mm. One-dimensional heat conduction was assumed for the cylinder part of the copper block. The heat flux is

$$q = -k_{Cu}\frac{dT}{dz} \tag{1}$$

where k_{Cu} is the thermal conductivity of copper, *z* is the coordinate normal to the copper surface. A least square correlation of temperatures versus *z* was written as $T = a_0 + a_1 z$, where a_0, and a_1 are coefficients correlated based on T_1, T_2, and T_3. The wall superheating degree ΔT is defined as $\Delta T = T_w - T_s$, where T_w is the wall temperature on the copper surface, T_s is the saturation temperature of ethanol at atmospheric pressure.

In Eq.1, the temperature gradient is replaced by

$$\frac{dT}{dz} = \frac{3T_1 - 4T_2 + T_3}{2\Delta z} \tag{2}$$

where Δz is the distance between two neighboring thermocouples.

Heat transfer coefficient was calculated as

$$h = \frac{q}{T_w - T_b} \tag{3}$$

where T_b is the bulk liquid temperature. Using the error propagation theory [22], the relative errors of heat flux *q* and heat transfer coefficients *h* are as follows:

$$\frac{\Delta q}{q} = \sqrt{\left[\left(\frac{\Delta k_{Cu}}{k_{Cu}}\right)^2 + \left(\frac{3\Delta T_1 \cdot k_{Cu}}{\Delta z \cdot q}\right)^2 + \left(\frac{4\Delta T_2 \cdot k_{Cu}}{\Delta z \cdot q}\right)^2 + \left(\frac{\Delta T_3 \cdot k_{Cu}}{\Delta z \cdot q}\right)^2 + \left(\frac{\delta(\Delta z)}{\Delta z}\right)^2\right]} \tag{4}$$

$$\frac{\Delta h}{h} = \sqrt{\left(\frac{\Delta q}{q}\right)^2 + \left(\frac{\Delta T_w}{T_w - T_b}\right)^2 + \left(\frac{\Delta T_b}{T_w - T_b}\right)^2} \tag{5}$$

Where $\delta(\Delta z)$ is the uncertainty of the distance of two neighboring thermocouples (Δz), here $\delta(\Delta z) = 0.02$ mm. The temperature measurements involved the uncertainty of 0.3 °C. Finally, we reached the uncertainties of heat flux and heat transfer coefficient of 4.50% and 4.66%, respectively.

3. Results and discussions

3.1. Boiling curves and heat transfer performance

Fig. 3 shows the comparison of boiling heat transfer performance on CS and SS. Following conclusions can be drawn: (i) At ONB, wall superheating $\Delta T = T_w$-T_s is ~5 K for SS and ~ 13 K for CS, indicating

Table 1
Physical properties of liquid metal Galinstan($Ga_{67}In_{20.5}Sn_{12.5}$)and water at 20 °C and 101.325 kPa.

fluids	ρ kg/m^3	T_m °C	T_s °C	h_{fg} kJ/kg	c_{pl} J/(kg·K)	λ W/(m·K)	$\mu \times 10^3$ Pa·s	$\sigma \times 10^3$ N/m	*Pr*
Water	998	0	100	2256.47	4184	0.6	1.002	72.8	7.008
Galinstan	6440	10.5	>1300	24.00	366	16.5	2.400	533.0	0.053

Table 2
Physical properties of ethanol at atmosphere pressure and 20 °C.

	T_s	ρ	h_{fg}	c_{pl}	λ	$\nu \times 10^6$	$\mu \times 10^3$	$\sigma \times 10^3$	Pr
	°C	kg/m^3	kJ/kg	kJ/(kg·K)	W/(m·K)	m^2/s	Pa·s	N/m	
Liquid	78.23	789.42	/	2.40	0.16	1.507	1.19	22.3	17.39
Vapor		1.65	849.63	1.72	0.02	6.061	0.010	/	0.861

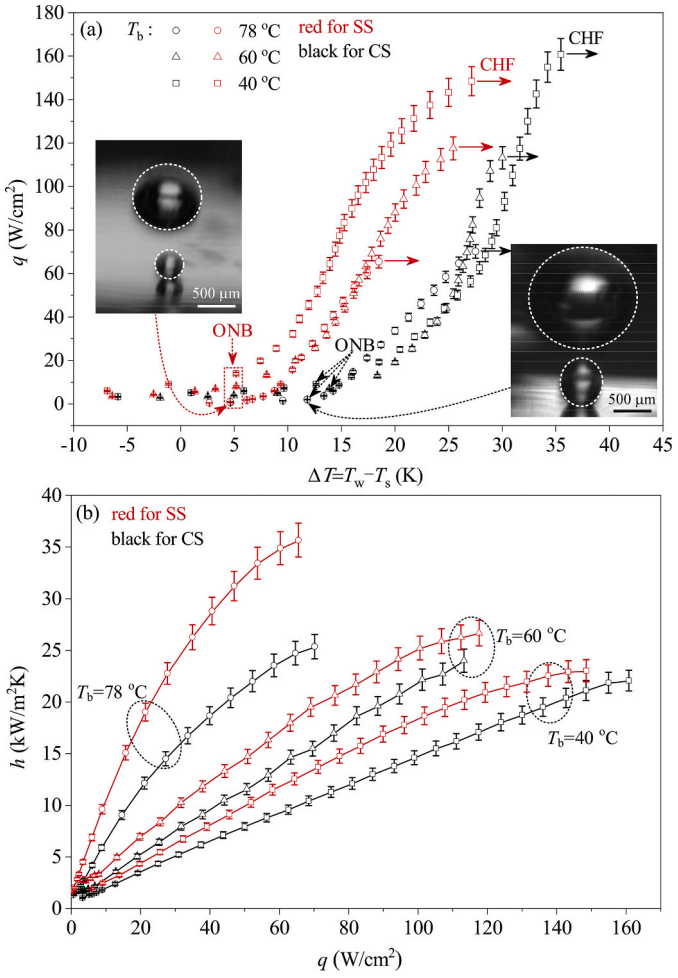

Fig. 3. Boiling curves (a) and heat transfer coefficients (b) on copper surface CS and soft surface SS. (The wall superheating at ONB on CS are 11.8 K, 13.9 K and 12.6 K for T_b = 78 °C, 60 °C and 40 °C, respectively. The wall superheating at ONB on SS are 4.6 K, 5.2 K and 5.2 K for T_b = 78 °C, 60 °C and 40 °C, respectively.)

easier triggering of boiling on SS, where T_w is the wall temperature and T_s is the saturation temperature of ethanol, noting that T_w is defined at the copper surface for boiling on both copper surface and soft surface. (ii) SS significantly enhances boiling heat transfer, increasing heat transfer coefficients h by 60.5% for saturated boiling with T_b = 78 °C, 36.6% for subcooled boiling with T_b = 60 °C and 30.5% with T_b = 40 °C, maximally. (iii) The difference of critical heat fluxes (CHFs) on CS and SS is weak on similar operating condition.

We explain the effect T_b on boiling heat transfer first. For saturated boiling, there is no condensation between growing bubble and pool liquid, generating enhanced disturbance of bubbles on liquid metal sublayer. In turn, the elastocapillary wave is enhanced to promote boiling heat transfer. The increase of pool liquid subcooling decreases bubble growth rate to weaken the intensity of elastocapillary wave, explaining larger heat transfer enhancement for saturated boiling than subcooled boiling. One is interest to the weak influence of SS on CHF. The key CHF mechanism is that vapor goes up vigorously at high heat flux, narrowing the liquid "channel" to supply liquid towards heater surface. Zuber assumed that CHF can be triggered, when the distance of neighboring vapor columns reaches the Kelvin-Helmholtz wavelength [23]. For present application, the elastocapillary wavelength is 269 μm, which is far away from the Kelvin-Helmholtz wavelength, explaining the weak effect of SS on CHF.

3.2. Heat transfer enhancement mechanisms

Fig. 4a shows the wrinkles structure on SS at q = 1.74 W/cm^2 and T_b = 78 °C (see Movie 1 in supplementary material). The intensity of surface wave is stronger when bubble is departing from SS than before and after the bubble departure. The wavelength is 269 μm and the wave propagation speed is 0.42 mm/s. The surface wave can be explained by both the energy analysis and force analysis. The former is considered first. Before departure, a bubble has a crown shape with a flat bottom interface contacting with heater surface, but after bubble departure, the bubble turns to be sphere to minimize the surface energy. The surface energy of bubble is larger before departure than after departure. Part of the residual surface energy is converted into the elastic potential energy of liquid metal. Solid has the concept of elasticity but liquid metal does not have such concept [24]. Even though the liquid metal is immersed in ethanol, weak oxidization of liquid metal exists to form a nanoscale shell to enclose liquid metal, absorbing the residual surface energy during bubble departure. The energy transfer from bubble to liquid metal is the energy source to drive the interface motion of liquid metal. The force analysis to deform liquid metal will be presented latter.

The interface wave generated by liquid metal enhances boiling heat transfer according to following mechanisms. First, the interface oscillating promotes the microconvection of thermal boundary layer of boiling liquid. In Fig. 4b-c, $\delta_{T,CS}$ and $\delta_{T,SS}$ refer to the thermal boundary layer of ethanol on copper surface and soft surface, respectively. Second, the interface oscillating ensures liquid renewal along horizontal plane. Third, the dynamic wrinkles of liquid metal provide larger surface area to enhance heat transfer between liquid metal and ethanol, acting as the fin effect. All these mechanisms are reflected by the decreased thermal boundary layer of ethanol. One notes that heat transfer coefficient h relates to thermal boundary layer as [25]:

$$\delta = 3.22\lambda/h \tag{6}$$

where λ is the thermal conductivity of ethanol. Now that h is experimentally determined in Fig. 3, δ is decided and plotted in Fig. 4c with log presentation, indicating obvious decrease of δ using soft liquid metal.

3.3. Elastocapillary wave and bubble dynamics

We need bubble dynamics parameters to identify the difference for the boiling on smooth copper surface and soft liquid metal surface. Boiling patterns are captured by a high-speed camera (MotionPro Y4, IDT, USA). The spatial resolution is 2.8 μm for each pixel. The visualization zone contains 1016 pixels by 1016 pixels, corresponding to an area of 2.85 mm by 2.85 mm. The recording rate of images was 4000 frames per second. Hence, the uncertainty for the bubble size measurement is 2.8 μm, and the bubble lifetime from nucleation to complete departure is 0.25 ms. For the statistical analysis of departure diameters of bubbles, about 12,000 frames of images were used, corresponding to a

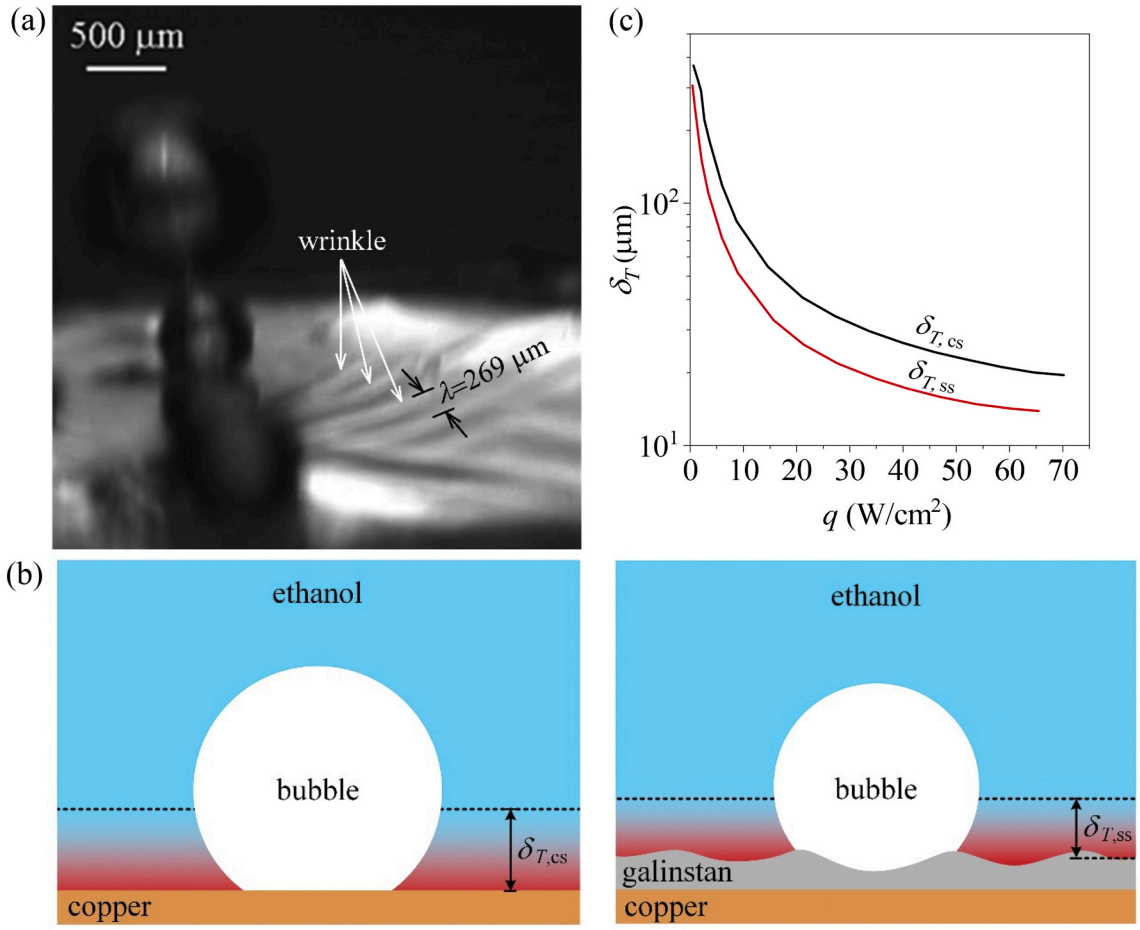

Fig. 4. Surface wave decreases thermal boundary layer thickness of ethanol (a: observation of surface wave at $q = 1.74$ W/cm^2, $T_b = 78$ °C and $\Delta T = 6.2$ °C; b: bubble growth in superheating thermal boundary layer on CS and SS; c: thermal boundary layer thickness versus heat fluxes on CS and SS for saturation boiling).

physical time of 3.0 s. Fig. 5 shows bubble dynamics at $q = 3$–4 W/cm^2. The similar heat flux corresponds to wall superheating $\Delta T = 13.4$ K on CS but 7.7 K on SS. We record the bubble lifetime before departure as τ and the diameter at departing state as D. The probability distributions of the two parameters are similar in shape on the two surfaces, but the quantitative data are quite different. For maximum probability, the copper surface holds $\tau = 41.05$ ms and $D = 1.02$ mm, but the soft surface holds $\tau = 6.07$ ms and $D = 0.53$ mm. SS not only increases bubble departure frequency by ~7 times, but also decreases bubble size by half (see Movies 2–3 corresponding to Fig. 5a-b and Fig. 5c-d respectively in supplementary material).

Various forces are applied on a bubble to influence its departure, among which buoyancy force F_b, Marangoni force F_m, surface tension force F_σ and others are the important ones [26]. For horizontally positioned surface, F_b is the driving force to separate a bubble from heater surface, but F_σ resists a bubble departure. Because surface tension depends on temperatures, the temperature gradient in pool liquid produces F_m, having downward direction to act as a resistance force. Now, attention is paid on F_σ. A bubble on flat surface is treated first (see Fig. 6a-b). The vertical component of surface tension force is:

$$F_{\sigma,y} = \pi D \gamma_{lv} \sin^2\theta \tag{7}$$

where D, γ_{lv} and θ are bubble diameter, surface tension between liquid and vapor of ethanol, and contact angle, respectively. Galinstan decreases θ for ethanol from 11.6° to 4.8°. Assuming identical D, $F_{\sigma,y}$ for SS is only 17.3% to CS, indicating significantly decreased resistance force for bubble departure. Bubble departs at a smaller size when enhancing surface wettability, agreeing with the contact angle effect reported in ref. [27].

Fig. 6c-f considers the practical condition under which contact point C is located on wrinkle surface, where α is the inclined angle of tangent line at point C with respect to horizontal position. Considering contact angle θ_{ss}, the surface tension force vector F_σ is neither along the wrinkle surface, nor normal to the wrinkle surface. For a bubble on the inner side of wrinkle, the vertical component of surface tension force is:

$$F_{\sigma,y} = F_\sigma \sin(\alpha + \theta_{SS}) \tag{8}$$

It has downward direction. When C is moving from wrinkle valley to apex, $F_{\sigma,y}$ decreases because α decreases from larger value to zero at apex (see Fig. 6d-e). When C arrives at the outer side of wrinkle, $F_{\sigma,y}$ switches the direction from downward to upward (see Fig. 6f). In one word, during the contact point traveling from inner side to outer side of wrinkle, the curved wrinkle switches the surface tension force in vertical component from the resistance role to the driving role, helping the bubble to depart from soft surface. Thus, bubble departs at smaller size and high frequency. One shall pay attention to the force interaction between bubble and liquid metal. During C moving from wrinkle valley to apex, as a counterforce, the vertical component of surface tension elevates liquid metal to increase wrinkle height, but it will collapse after bubble departure. Such disturbance propagates along horizontal plane to generate elastocapillary wave such as shown in Movie 1 in supplementary material.

We note that our present analysis regarding the bubble interaction with the soft liquid metal surface is based on the characteristic contact angle which is measured on plain surfaces. It is a complicated phenomenon for the contract angle concept in a boiling system. Recently,

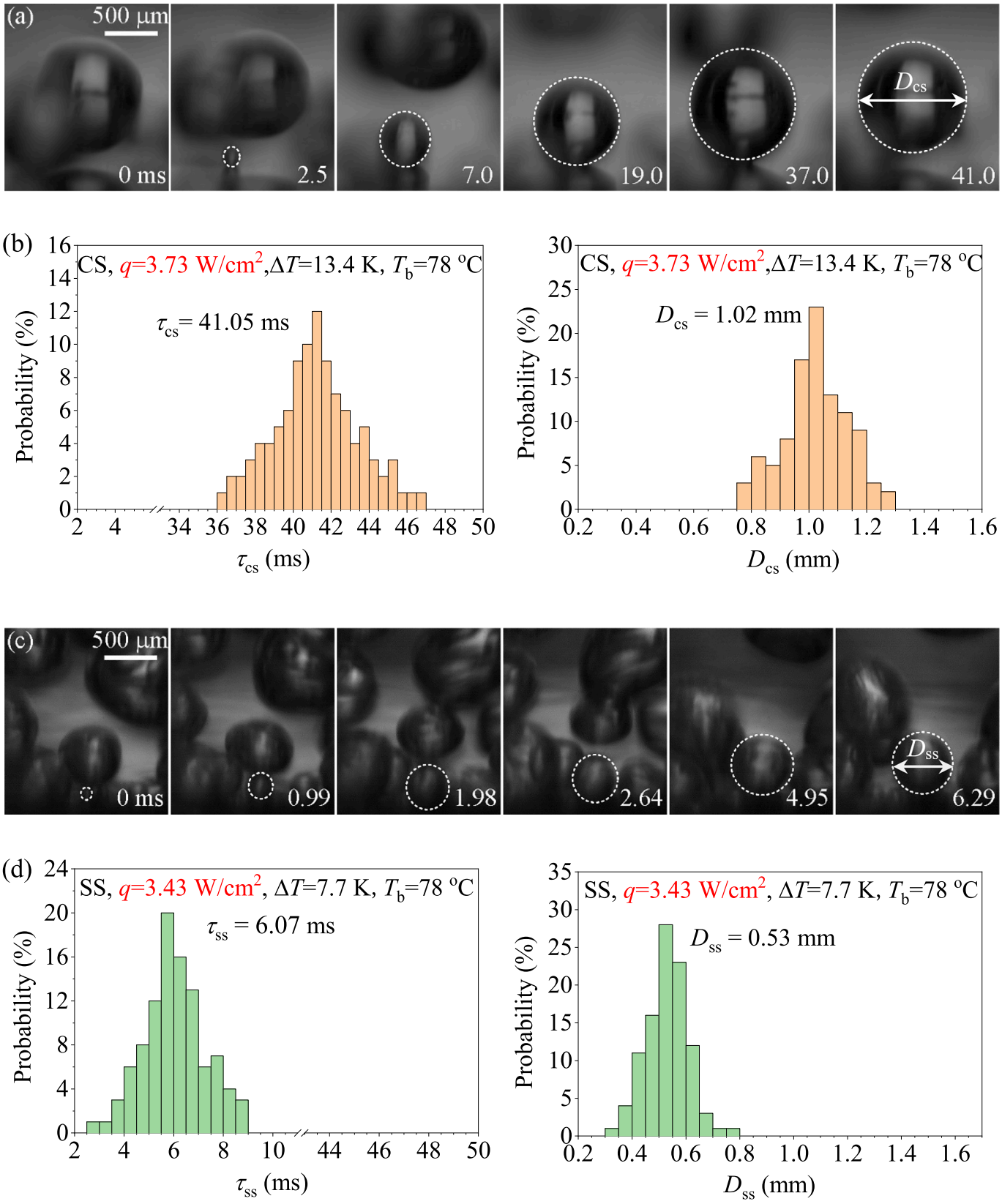

Fig. 5. Bubble dynamics near ONB (a: bubble images near ONB on CS; b: probabilities for bubble lifetime and departure diameter on CS; c: bubble images near ONB on SS; d: probabilities for bubble lifetime and departure diameter on SS).

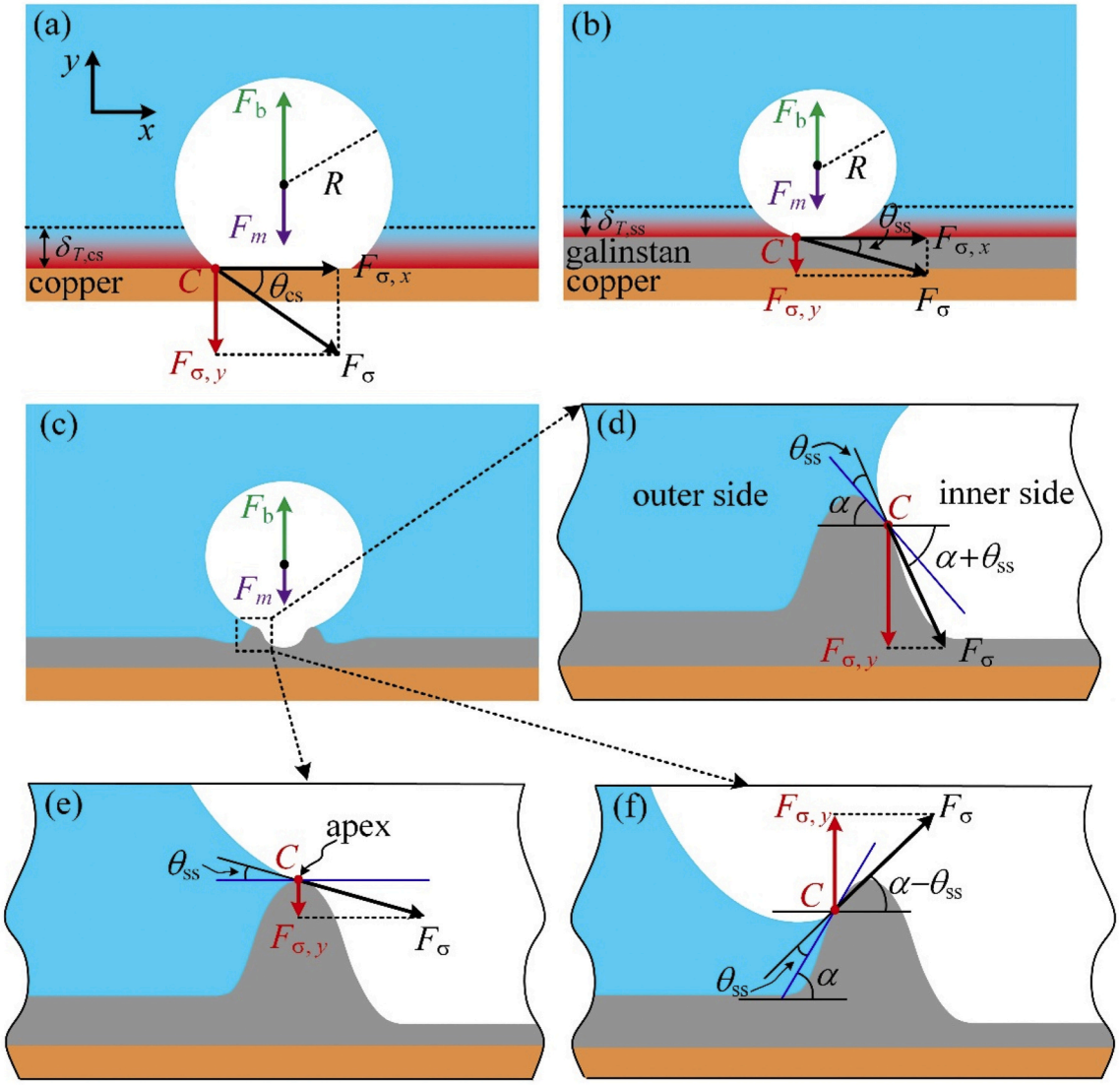

Fig. 6. The competition between buoyancy force, Marangoni force and surface tension to dominate bubble departure (a: bubble on CS; b: bubble on plain liquid metal surface; c: bubble on waved liquid metal surface; d, e & f: surface tension force on the three locations of wrinkle).

several articles referred to the concepts of macro contact angle and micro contact angle [28–30]. The characteristic contact angle just like used in Fig. 6 is actually the macro contact angle. In these studies [28–30], micro contact angle is supposed to occur neat the contact line of three phases of vapor-liquid-solid. When bubble nucleation just takes place, strong liquid evaporation near the contact line results in a micro contact angle which is larger than 90^o. Following then, the micro contact angle will decrease and may approach the macro contact angle, due to the energy minimization of the bubble system. During bubble growth, macro contact angle may also change due to the hysteresis phenomenon: it decreases when liquid recedes and increases when liquid advances. It is noted that micro contact angle is just a hypothesis during bubble growth, which has not been verified by experiment. In this study, boiling is treated on a liquid metal surface, not on a solid wall surface. Hence, the micro contact angle analysis is not incorporated in this study, but will be paid attention in the future.

Finally, we discuss bubble nucleation on soft surface. It is observed that following a larger bubble (for example, ~0.5 mm in diameter) departure, consecutive miniature bubbles quickly nucleate and depart from the surface, which are evidenced by bubbles a and b in Fig. 7a and Movie 4 in supplementary material. During the larger bubble departure, a seed bubble in the liquid metal cavity is separated from its mother bubble by neck breaking (see Fig. 7b). Our study shows that the easier bubble nucleation and departure decrease wall superheating at ONB from ~13 K on hard copper surface to ~5 K on soft liquid metal surface. Rykaczewski and Phadnis [31] theoretically evaluated whether softening of the surface could control wall superheating at onset of nucleate boiling. They gave the theoretical expression for the vapor embryo formation rate for interface of a volatile liquid such as ethanol (represented by subscript 1), with liquid-vapor surface tension γ_1 on a nonvolatile liquid such as Galinstan (represented by subscript 2) with liquid-vapor surface tension γ_2. Jarvis et al. [32] showed that bubble nucleation at the interface of the two liquids will only occur when the interfacial tension between the two liquids of γ_{12}, is greater than both $\gamma_2 - \gamma_1$ and $\gamma_1 - \gamma_2$. The way to ensure both criteria is to assume a hypothetical liquid substrate family with $\gamma_1 = \gamma_2$ and varied γ_{12}. The theoretical predictions show that the wall superheating for ethanol boiling could decrease by 5 K, while the present experiment demonstrates that such superheating is decreased from ~13 K on hard surface to ~5 K on soft surface. But any way, the prediction by Rykaczewski and Phadnis qualitatively agrees with our present observations. Rykaczewski and Phadnis [31] also hypothesized that softening of the substrate augments

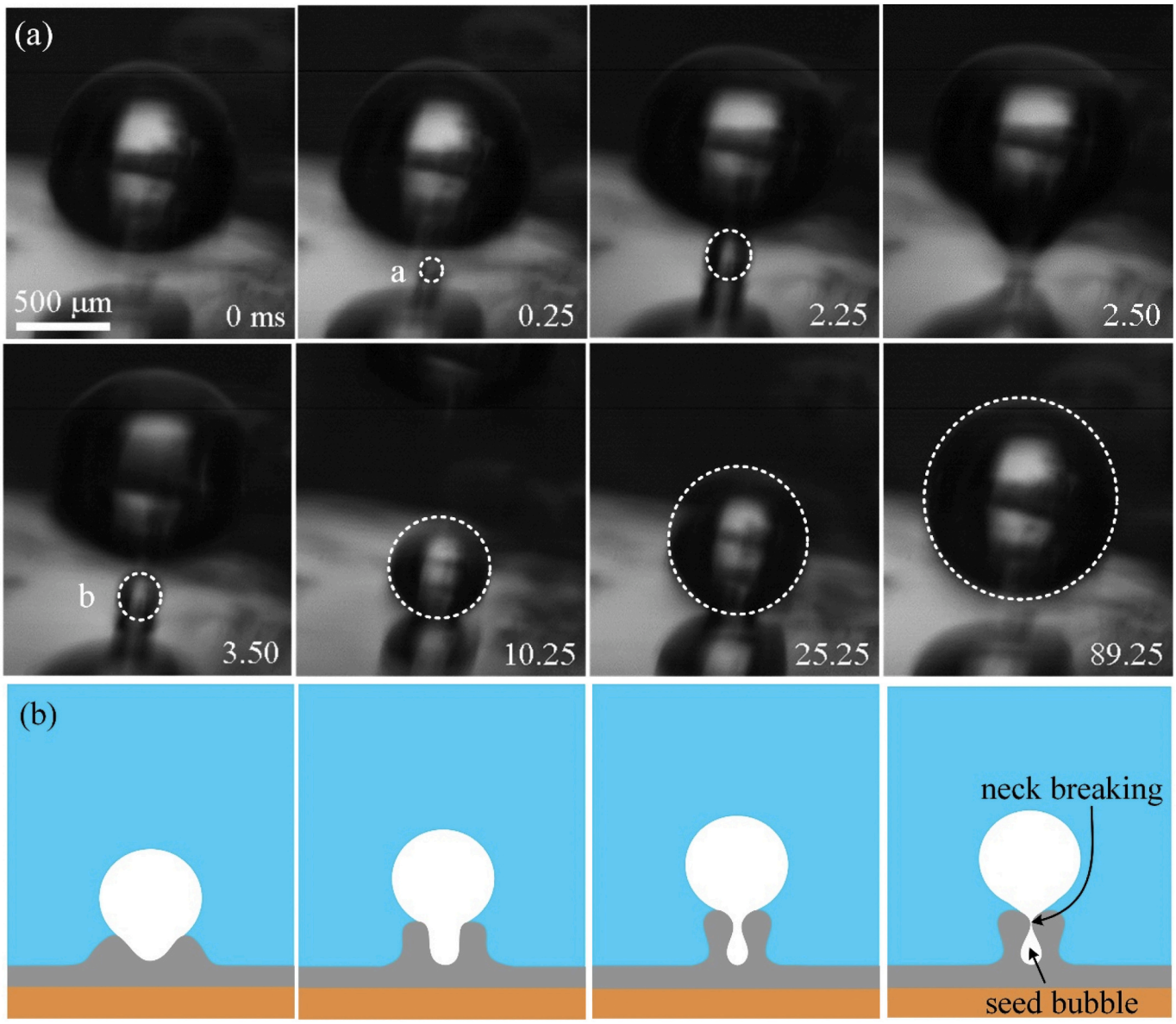

Fig. 7. A bubble departure triggers a seed bubble inside a cavity within SS (a: photos given at $q = 0.91$ W/cm^2, $T_b = 78$ °C and $\Delta T = 4.6$ K; b: dynamic formation of seed bubble in the cavity within SS during bubble departure).

ONB through a vapor trapping mechanism stemming from bridging of the cavities by microscopic deformation. The cavity bridge is driven by the vertical component of the liquid's surface tension competed with the shear modulus of soft material, scaled as the elastocapillary length.

4. Conclusions

In summary, we spread a thin soft layer of liquid metal on a hard substrate to alter the behavior of superheating boundary layer of boiling liquid. We show that, wall superheating at ONB decreases from ~13 K on hard surface to ~5 K on soft surface. The soft surface increases bubble departure frequency by ~7 times and reduces bubble departure size by half, corresponding to a maximum 60.5% heat transfer increasement for saturated boiling of ethanol. The elastocapillary wave is self-activated by energy conversion from departing bubble to soft mater. Dynamic wrinkles are caused by the vertical component of surface tension on soft mater. The interface instability decreases the effective boundary layer thickness of boiling liquid. The easier bubble nucleation is explained by the bubble nucleation theory with a violate liquid contacting with a non-volatile liquid. This is a preliminary work regarding boiling on soft surface, the underlying mechanism needs further investigation.

Declaration of Competing Interest

The authors declare that they have no known competing financial interests or personal relationships that could have appeared to influence the work reported in this paper.

Acknowledgement

We appreciate the funding support from the National Natural Science Foundation of China (No. 51821004 and 51806065) and Fundamental Research Funds for Central Universities (No. 2020DF002).

Appendix A. Supplementary data

Supplementary data to this article can be found online at https://doi.org/10.1016/j.icheatmasstransfer.2020.105019.

References

[1] L. Chen, E. Bonaccurso, T. Gambaryan-Roisman, V. Starov, N. Koursari, Y. Zhao, Static and dynamic wetting of soft substrates, Curr. Opin. Colloid Interface Sci. 36 (2018) 46–57.

[2] S.J. Park, B.M. Weon, J.S. Lee, J. Lee, J. Kim, J.H. Je, Visualization of asymmetric wetting ridges on soft solids with X-ray microscopy, Nat. Commun. 5 (2014) 4369.

[3] Y. Yu, Substrate elastic deformation due to vertical component of liquid-vapor interfacial tension, J. Appl. Math. Mech. 33 (9) (2012) 1095–1114.

[4] E.R. Jerison, Y. Xu, L.A. Wilen, E.R. Dufresne, Deformation of an elastic substrate by a three-phase contact line, Phys. Rev. Lett. 106 (18) (2011), 186103.

[5] R. Pericet-CaMara, A. Best, H.J. Butt, E. Bonaccurso, Effect of capillary pressure and surface tension on the deformation of elastic surfaces by sessile liquid microdrops: an experimental investigation, Langmuir 24 (19) (2008) 10565–10568.

[6] B. Li, Y.P. Cao, X.Q. Feng, H. Gao, Mechanics of morphological instabilities and surface wrinkling in soft materials: a review, Soft Matter 8 (21) (2012) (5728–5720).

[7] Q. Liu, T. Ouchi, L. Jin, R. Hayward, Z. Suo, Elastocapillary crease, Phys. Rev. Lett. 122 (9) (2019), 098003.

[8] A. Chakrabarti, M.K. Chaudhury, Direct measurement of the surface tension of a soft elastic hydrogel: exploration of Elasto-capillary instability in adhesion, Langmuir. 29 (23) (2013) 6926–6935.

[9] B. Roman, J. Bico, Elasto-capillarity: deforming an elastic structure with a liquid droplet, J. Phys. Condens. Matter 22 (49) (2010), 493101.

[10] C. Py, R. Bastien, J. Bico, B. Roman, A. Boudaoud, 3D aggregation of wet fibers, Europhys. Lett. 77 (2007) 44005.

[11] J. Bico, B. Roman, L. Moulin, A. Boudaoud, Elastocapillary coalescence in wet hair, Nature. 432 (7018) (2004) 690.

[12] J.A. Zimberlin, N. Sanabria-Delong, G.N. Tew, A.J. Crosby, Cavitation rheology for soft materials, Soft Matter 3 (6) (2007) 763–767.

[13] Q. Wang, M. Tahir, J. Zang, X. Zhao, Dynamic electrostatic lithography: multiscale on-demand patterning on large-area curved surfaces, Adv. Mater. 24 (15) (2012) 1947–1951.

[14] J. Gerber, T. Lendenmann, H. Eghlidi, T.M. Schutzius, D. Poulikakos, Wetting transitions in droplet drying on soft materials, Nat. Commun. 10 (1) (2019) 1–10.

[15] S. Mangili, C. Antonini, M. Marengo, A. Amirfazli, Understanding the drop impact phenomenon on soft PDMS substrates, Soft Matter 8 (39) (2012) 10045–10054.

[16] Jinliang Xu, Xiongjiang Yu, Wu Jin, Porous-wall microchannels generate high frequency “eye-blinking” interface oscillation, yielding ultra-stable wall temperatures, Int. J. Heat Mass Transf. 101 (2016) 341–353.

[17] X. Ji, J. Xu, H. Li, G. Huang, Switchable heat transfer mechanisms of nucleation and convection by wettability match of evaporator and condenser for heat pipes: Nano-structured surface effect, Nano Energy 38 (2017) 313–325.

[18] W. Li, Z. Wang, F. Yang, T. Alam, M. Jiang, X. Qu, F. Kong, A.S. Khan, M. Liu, M. Alwazzan, Y. Tong, C. Li, Supercapillary architecture-activated two-phase boundary layer structures for highly stable and efficient flow boiling heat transfer, Adv. Mater. 32 (2) (2019) 1905117.

[19] S.G. Kandlikar, Controlling bubble motion over heated surface through evaporation momentum force to enhance pool boiling heat transfer, Appl. Phys. Lett. 102 (5) (2013), 051611.

[20] S. Xu, B. Yuan, Y. Hou, T. Liu, J. Fu, J. Liu, Self-fueled liquid metal motors, J. Phys. D. Appl. Phys. 52 (35) (2019).

[21] Q. Wang, Y. Yu, J. Liu, Preparations, characteristics and applications of the functional liquid metal materials, Adv. Eng. Mater. 20 (5) (2018), 1700781.

[22] A. Jaikumar, S.G. Kandlikar, Enhanced pool boiling heat transfer mechanisms for selectively sintered open microchannels, Int. J. Heat Mass Transf. 88 (2015) 652–661.

[23] N. Zuber, Hydrodynamic Aspects of Boiling Heat Transfer, PhD Thesis, University of California, Los Angeles, CA, 1959.

[24] A. Koh, R. Mrozek, G. Slipher, Characterization and manipulation of interfacial activity for aqueous Galinstan dispersions, Adv. Mater. Interfaces 5 (5) (2018), 1701240.

[25] C.L. Tien, A hydrodynamic model for nucleate pool boiling, Int. J. Heat Mass Transf. 5 (6) (1962) 533–540.

[26] X. Wang, Z. Wu, J. Wei, B. Sunden, Correlations for prediction of the bubble departure radius on smooth flat surface during nucleate pool boiling, Int. J. Heat Mass Transf. 132 (2019) 699–714.

[27] Y. Nam, E. Aktinol, V.K. Dhir, Y.S. Ju, Single bubble dynamics on a superhydrophilic surface with artificial nucleation sites, Int. J. Heat Mass Transf. 54 (7–8) (2011) 1572–1577.

[28] H.T. Phan, N. Caney, P. Marty, S. Colasson, J. Gavillet, A model to predict the effect of contact angle on the bubble departure diameter during heterogeneous boiling, International Communications in Heat and Mass Transfer 37 (8) (2010) 964–969.

[29] H.T. Phan, N. Caney, P. Marty, S. Colasson, J. Gavillet, Surface wettability control by nanocoating: the effects on pool boiling heat transfer and nucleation mechanism, Int. J. Heat Mass Transf. 52 (23–24) (2009) 5459–5471.

[30] E. Teodori, T. Valente, I. Malavasi, A.S. Moita, M. Marengo, A.L.N. Moreira, Effect of extreme wetting scenarios on pool boiling conditions, Appl. Therm. Eng. 115 (2017) 1424–1437.

[31] K. Rykaczewski, A. Phadnis, Could use of soft surfaces augment onset of nucleate boiling? Nanoscale Microscale Thermophys. Eng. 22 (3) (2018) 230–238.

[32] T.J. Jarvis, M.D. Donohue, J.L. Katz, Bubble nucleation mechanisms of liquid droplets superheated in other liquids, J. Colloid Interface Sci. 50 (2) (1975) 359–368.